Adsorption of Rare Earth Elements in DNA functionalized Mesoporous Carbon

Colin E. Unsworth¹, Chin Chen Kuo², Alexei Kuzmin³, Syed Khalid⁴, Dipendu Saha^{1,*}

- **1**. Chemical Engineering Department, Widener University, 1 University Place, PA 19013, USA.
- **2**. Advanced Materials Characterization Laboratory, University of Delaware, Newark, DE 19716, USA,
- **3**. Institute of Solid State Physics, University of Latvia, Kengaraga street 8, LV-1063, Riga, Latvia,
- 4. NSLS-II, Brookhaven National Laboratory, Rochester Ave, Upton, NY 11973

^{*}Corresponding author's e-mail: <u>dsaha@widener.edu</u>, <u>dipendus@gmail.com</u> Phone: +1 610 499 4056, Fax: +1 610 499 4059

Abstract:

Recovery and separation of rare earth elements (REEs) are of national importance owing to the specific usages, high demand and low supply of these elements. In this research, we have investigated the adsorption of rare earth elements in DNA functionalized mesoporous carbons with a BET surface area of 605 m²/g and median mesopore width 48 Å. Three types of single-stranded DNA, one with 100 base units of thymine, other with 20 units of thymine and thirdly, a 2000-unit long DNA from salmon milt were grafted on the carboxylated mesoporous carbon surface. All the DNA functionalized mesoporous carbons demonstrated higher adsorption of REEs compared to pristine mesoporous carbon and DNA grafted with 100 units of thymine demonstrated slightly higher adsorbed amounts compared to others. Pure neodymium (Nd(III)) adsorption in aqueous phase demonstrated an adsorbed amount of 110.4 mg/g with respect to the initial concentration of 500 mg/g. pH variation study with pure Nd(III) demonstrated that the adsorbed amount is higher at elevated pH compared to that of lower pH thereby suggesting possible recovery at lower pH. Adsorption of a mixture of 16 REEs, including Sc, Lu, Tm, Yb, Er, Ho, Tb, Dy, Y, Eu, Gd, Sm, Ce, Nd, Pr and La revealed that adsorbed amount increased with the increase in atomic weight and metallic radii of elements within the lanthanides. Calculation of the distribution coefficients for all the equilibrium adsorption amounts suggested that adsorption is more effective in the lower concentration region. The Nd L₃-edge X-ray absorption near edge structure (XANES) confirmed a 3+ oxidation state of Nd in the adsorbed phase. Extended X-ray absorption fine structure (EXAFS) confirmed the local atomic structure relaxation of Nd-complexes in the adsorbed phase and shortening of Nd-O bond distance by about 0.03-0.04 Å, that may be associated with its local complexation at the carbon surface.

Keywords: Rare earth element (REE); Mesopoorus carbon; DNA; Adsorption; X-ray absorption spectroscopy (XAS)

1. Introduction

Rare earth elements (REEs) or rare earth metals (REMs) are seventeen elements of the periodic table including fifteen lanthanides, scandium and yttrium. In a broad spectrum, the rare earth elements can be classified into the two general categories of light and heavy rare-earths with varying degrees of demands and utilization¹. Light rare-earths include lanthanum (La), cerium (Ce), praseodymium (Pr), neodymium (Nd) and samarium (Sm) whereas heavy rare-earths consist of europium (Eu), gadolinium (Gd), terbium (Tb), dysprosium (Dy), holmium (Ho), erbium (Er), thulium (Tm), ytterbium (Yb), lutetium (Lu) and yttrium (Y). Heavy rare-earths have slightly more economic values and less available. The majority of these elements have specific yet widespread utilization in wide spectra of electronics, phosphors and optical devices, permanent magnets, power sources and different other military applications². Additionally, a more significant fraction of REEs is termed as either critical or energy critical elements owing to their critical role in energy sectors. They are not mined, processed or traded in large quantities. As of today's scenario, 95% of the world's supply of REEs is controlled by one to two countries, and recent export restriction of REEs from those countries put the other countries, including the USA at the risk of interrupted supplies of these elements³. In addition to increasing conventional mining, waste stream recovery of REEs is an accepted strategy to maintain the supply-demand balance. Among the pool of REEs, neodymium (Nd) is one of the highly important rare earth elements. Because of its unusually high heat capacity, Nd is used in cryocoolers. The most important use of Nd is to make the strongest permanent magnets. Because of its performance, the global demand for Nd may grow as high as 700 % in the next two decades⁴. Recovery and recycling of few REEs, like neodymium (Nd) and dysprosium (Dy) from the waste NdFeB magnets is one of the key REE separation needs of today⁵.

The rare earth elements possess very similar chemical properties with each other and with other neighboring elements of the periodic table and therefore it is challenging to separate them. Solvent extraction with a specific type of solvents is the most up-to-date commercially available technology to enrich REEs from their ores^{6,7,8,9,10,11}. Although solvent extraction is commonly used in the purification of REEs from their ores, it is not effective in extracting the low concentrations of REEs found waste streams. Additionally, solvent extraction is considered hazardous owing to the involvement of a large amount of toxic solvents¹². It is also time-consuming, labor-intensive and may leave undesired residues¹³,¹⁴,¹⁵. Contrary to solvent extraction, the adsorption-based separation process is regarded as sustainable, benign and inexpensive compared to almost all other processes that have been employed to recover REEs. Besides physisorption in nanoporous materials, it has also been demonstrated that phosphorous and oxygen-based functionalities on the adsorbent surface facilitate the capture of rare earths. In adsorbent-based systems, phosphoric acid functionalized silica-based adsorbents were employed for the adsorption of Nd, Eu, Er and Y, although the exact role of phosphorous was not investigated ¹⁶. Our previous research demonstrated a higher uptake of Nd and Dy compared to Fe(III) in phosphorous functionalized microporous carbon¹⁷. Cell walls of different types of natural or genetically modified bacteria were employed for the capture of various REEs and it was hypothesized that the phosphate functionality on the cell wall of bacteria strains is responsible for the affinity-based capture of those rare-earth elements¹⁸,¹⁹. Recently, commercially available DNA-based materials were employed to selectively capture REEs through their phosphorous

and oxygen functionalities. Freeze-dried and powdered salmon milt as a source of DNA was employed to adsorb 15 REEs in a column process²⁰. The same research group also reported cross-linking of DNA with cellulosic filter paper by N,N'-disuccinimidyl suberate, and DNA-filter hybrid material was used to adsorb Nd, Dy and Lu from aqueous solutions²¹. In the last two research papers that demonstrated the feasibility of DNA functionalities in separating REEs, the authors also reported the *in–situ* L₃-edge extended x-ray absorption fine structure (EXAFS) analysis to investigate the binding of few REEs (Dy and Lu) with phosphorus and oxygen functionalities^{20,21}.

Despite the fact that the affinity of REEs with phosphorous has been illustrated in the literature and DNA has been employed as a source of that functionality, the key issue of these studies was the control and quantification of phosphorous functionalities on the sorbent surface. Furthermore, the low surface area of the host material restricted sufficient functionalization of phosphorous functionality that ultimately limited the overall uptake of REEs. In this research, we have chemically grafted a few specific sequences of single-stranded DNA onto the carboxylated and soft-templated mesoporous carbon surface. We have studied the adsorption behavior of 16 rare earth elements from their mixtures and specifically studied the adsorption equilibrium and kinetics of neodymium onto the DNA grafted carbon. We also studied the binding nature of REEs with X-ray absorption spectroscopy (XANES/EXAFS).

2. Experimental

- 2.1 Synthesis of single-stranded DNA grafted mesoporous carbon
- (a) Synthesis of soft-templated mesoporous carbon

The soft-templated mesoporous carbons were synthesized based on our previous publications²²,²³,²⁴. Typically, 5 g of resorcinol (Sigma-Aldrich) was added to the surfactant, Pluronic F127TM, (BASF), along with 12.5 mL of ethanol and 12.5 mL of deionized water. The mixture was then acidified with 5 mL of 37% (v/v) hydrochloric acid (HCl) and left under continuous stirring conditions overnight. After that, 5 mL of 37% (v/v) formaldehyde (HCHO) was added as a cross-linking agent. The mixture was again left under continuous stirring conditions overnight, to allow complete polymerization. The remaining transparent liquid solution was separated by decanting, while the white polymer layer was spread on to a petri dish and allowed to sit for three days to cure the polymer further. After curing, the polymer was placed in a porcelain boat, which was inserted into a Lindberg/Blue MTM tube furnace and heated to carbonize the sample. The furnace was heated to $100 \, ^{\circ}C$ at a rate of $10 \, ^{\circ}C \cdot min^{-1}$, followed by heating to $400 \, ^{\circ}C$ at a rate of $2 \, ^{\circ}C \cdot min^{-1}$, and then heating to $850 \, ^{\circ}C$ at a rate of $10 \, ^{\circ}C \cdot min^{-1}$. After that, it was cooled to room temperature and taken out. All the heating and cooling operations were performed under N₂ gas flow.

(b) Carboxylation of mesoporous carbons

To carboxylate the mesoporous carbons, 1 g of mesoporous carbon was mixed with 45 mL of concentrated H_2SO_4 and 15 mL of concentrated HNO_3 . This mixture was then heated to 50 °C for 5 hours in a round bottom flask. Afterward, the carbon powder was separated from the liquid and washed several times with copious amounts of deionized water. The carbon was then ultrasonicated for 10 minutes, rewashed with more deionized water, and dried.

(c) DNA grafting

Three types of DNA were chosen to be grafted onto the pristine mesoporous carbon, (i) a custom made single-stranded oligo with 20 thymine units and amino C6 linker in the 5' end and phosphate (PO_4^-) groups at the 3' end (Eurofins), (ii) A custom made singlestranded oligo with 100 thymine units and amino C6 linker in the 5' end and phosphate (PO_{\perp}^{-}) groups at the 3' end (ThermoFisher), and (iii) commercially available DNA extracted from salmon tastes with a length equivalent to 2000 base pairs in salt form (Sigma-Aldrich). Both custom synthetic DNA sources are single-stranded amine-terminated DNA sources. The fish DNA, however, is double-stranded and thus was heated to 100 °C for 10 minutes to convert it to a single-strand. The thymine unit was chosen as the only base for the single stranded DNA because it is the only base with a secondary amine group and hence is not expected to react with carboxylate groups attached with the mesoporous carbon, essentially signifying that only the terminal primary amine group (-NH₂) will react and be grafted on mesoporous carbons. Typically, $8.75 \mu L$ of DNA solution was mixed with $10.0 \, mL$ of biological grade, ultrapure water (Sigma Aldrich), without any buffer, added to 1.00 g of carboxylated mesoporous carbon, continuously stirred for 1 hour, and then frozen at -20 °C overnight. The following morning, the frozen suspension was thawed, washed with copious amounts of ultrapure water, filtered, and dried. The mesoporous carbons grafted with 20 units thymine, 100 units thymine, and salmon testes DNA are termed as MC-T20, MC-T100, and MC-fish, respectively. The resulting carbons were consistently preserved at -20 °C, being only removed from the freezer briefly when used for laboratory testing. The overall schematic of the synthesis of DNA grafted carbon is shown below in figure 1.

2.2 Characterization of mesoporous carbon

The porosity of pure mesoporous carbon was measured by N_2 adsorption at 77 K and CO_2 adsorption at 273 K. We could not perform porosity measurements for DNA grafted carbons as we could not outgas the samples prior to adsorption measurements. Outgassing procedures at elevated temperature for prolonged temperature would have degraded the DNA fragments. The Brunauer-Emmett-Teller (BET) surface area was calculated from the N_2 adsorption plot, whereas the pore size distribution plot was obtained from non-local density functional theory (NLDFT) by using instrument software and N_2 and CO_2 adsorption data. The high-resolution Scanning Electron Microscopy (HR-SEM) images and the corresponding energy-dispersive X-ray (EDX) maps of MC-T100 were obtained in JEOL 7500F HRSEM instrument with 15 kV potential and 85,000 magnification. To further visualize phosphate group in SEM-EDX, we also reacted the MC-T100 sample with 1% uranyl acetate solution as it can chelate with phosphate groups of DNA thereby making them better visible. MC-T100 was ultrasonicated with the solution for 10 minutes and then washed with DI water several times and stored at -4 °C until used for imaging.

2.3 Adsorption of rare earth elements

MC, MC-T20, MC-T100, and MC-fish were tested for their ability to adsorb Nd(III) from the solution. An aqueous solution of neodymium nitrate hexahydrate $(Nd(NO_3)_3 \cdot 6H_2O)$ was prepared at a concentration of $10 \, mg/L$ with respect to neodymium. For each sorbent, approximately $25 \, mg$ of sorbent was dispensed into $25 \, mL$ of $Nd(NO_3)_3 \cdot 6H_2O$ solution and left continuous stirring in a round bottom flask for two hours. Afterward, the carbon sorbents were removed through filtration and the remaining concentration of Nd(III)

was measured employing inductively coupled plasma mass spectroscopy (ICP-MS, ThermoFisher). Each test is run triplicate and all studies were repeated twice, with average values reported with standard deviation as error bars. In the course of this study, it was found that MC-T100 extracted the greatest amount of Nd(III) (detailed results are shown in the results and discussion section), all the other studies were performed with that adsorbent only.

2.4 Pure Nd adsorption

Equilibrium and kinetic studies of pure Nd(III) were performed with MC-T100 only. In order to perform the equilibrium studies, 25 mL Nd(III) solutions of concentrations of 71, 127, 190, 252, 378, 504 *mg/L* were each stirred with 25 mg MC-T100 for two hours. After that, the carbon was separated by filtration and the remaining concentration of Nd(III) was measured by ICP-MS analysis. To perform kinetics studies, 25 ml 500 mg/L Nd(III) solution was employed within the time interval of 10 mins, 30 mins, 1 hr, 2 hr and 3 hrs. The analysis of residual Nd in all the runs was also performed by ICP-MS and adsorbed amounts were calculated by difference. The feasibility of pH swing adsorption as a means of recovering adsorbed Nd and regenerating the DNA grafted mesoporous carbon, post adsorption, was investigated by measurements of the effect of pH on the amount of Nd(III) in the adsorbed phase at equilibrium. To this end, $100 \, mL$ samples of a $500 \, mg/L$ Nd(III) solution, made from $Nd(NO_3)_3 \cdot 6H_2O$, were pH adjusted by addition of either nitric acid (HNO_3) or sodium hydroxide (NaOH), with pH measured by Orion Star A215 pH/conductivity meter (Thermo Scientific). pH values ranged from 1.72 to 8.06; higher pH values produced a sodium nitrate precipitate and hence were not tested. 25 mg of MC-T100 was added to 25 mL of each of the

pH adjusted solutions, and left under continuous stirring for 2 hours; afterward, the carbon sorbent was filtered out, and the concentration remaining in solution was measured by ICP-MS, using 10 ppb Sn with m/z number of 118 (sigma 96215) as internal standard since it is compatible and has limited interference to all REEs. In addition to that, the m/Z number is close to most of REEs for better precision. A trial has done before formal analysis and the stability ratio of Sn118 is ranged from 90-120%. The test with ratio below 90% or higher than 120% will be excluded and rerun. Again, duplicates of each trial were performed, with standard deviation reported as error bars.

2.5 REE mixture test

To perform the REE mixture tests, an initial mixture consisting of 16 REEs (Sigma Aldrich), including Sc, Lu, Tm, Yb, Er, Ho, Tb, Dy, Y, Eu, Gd, Sm, Ce, Nd, Pr and La (50 mg/L with respect to each element) was employed. Only equilibrium adsorption analyses were performed with the initial concentration of 1 and 30 ppm with respect to each element. The residual concentration analysis of each element in the mixture was performed by ICP-MS (Thermo Fisher).

2.6 X-Ray Absorption Spectroscopy (XAS)

The bonding nature of Nd(III) on the MC-T100 sorbent was investigated by x-ray absorption spectroscopy (XAS). 250 mL of a 1000 mg/L solution of Nd(III), made from $Nd(NO_3)_3 \cdot 6H_2O$, was brought into contact with MC-T100 under continuous stirring conditions for two hours. The sorbent was then removed by filtration and dried. X-ray absorption spectra of Nd(III) nitrate hexahydrate $(Nd(NO_3)_3 \cdot 6H_2O)$ and Nd(III) adsorbed on

mesoporous carbon were recorded at National Synchrotron Light Source II (NSLS-II) beamline QAS of Brookhaven National Laboratory (BNL). The synchronized radiation was monochromatized using Si(111) monochromator, and using 40 % detuning in order to eliminate higher harmonics, mostly third, as second is almost absent by the virtue of the crystal. Its intensity before the sample was measured using an ion chamber, and after the sample was measured in both modes of operation, transmission and fluorescence. In the transmission mode ion chamber was used, and in the fluorescence mode PIPS (Passivated Implanted Planar Silicon) large diode detector was used. However, for data analysis, only transmission mode was used. All the spectral measurements were performed at room temperature. The average over 20 spectra was used for solid Nd(NO₃)₃·6H₂O powder and over 9 spectra for Nd in mesoporous carbon. Chromium foil was used to calibrate the energy scale of the monochromator.

3. Results and Discussion

3.1 Characteristics of DNA grafted mesoporous carbons

The N_2 adsorption-desorption plot at 77 K is shown in the *inset* of figure 2. The isotherm represents a type IV nature according to the IUPAC nomenclature. The hysteresis loop signifies the presence of mesopore. The BET surface area of the mesoporous carbon is $605 \text{ m}^2/\text{g}$ as obtained from N_2 adsorption isotherm. As observed in the pore size distribution, (figure 2), the mesopore width is about 48 Å, whereas the carbon also has few micropore widths, centered around 5, 9 and 15 Å. This carbon also has a total pore volume of 0.56 cm³/g.

The high-resolution SEM image of MC-T100 is shown in figure 3(a) and the corresponding element distribution maps for carbon, nitrogen, oxygen, phosphorous and

uranium are shown in figure 3(b) to (f). As evident, carbon is the most dominant element and shows its highest intensity and number of pixels. Oxygen is the next dominant element and originates from the mesoporous carbon surface, carboxylated functionalities and DNA structures. As observed in the figure, there are significant amounts of the nitrogen atoms in the carbon matrix that have only been contributed from the bases of DNA strand (amino C6-T100-PO₄). The pixels signifying phosphorous atom have also originated from the same DNA strand whereas the pixels for uranium originated from the uranyl-phosphate complex that was generated prior to SEM imaging to better visualize the phosphorus atoms under EDX.

3.2 Adsorption of rare earth elements

The best adsorbent data is shown in figure 4. It is observed that the mesoporous carbon grafted with 100 units of oligo, MC-T100, demonstrated highest Nd(III) adsorption, which is about 9.8 mg/g when the initial concentration was 10 mg/L. The adsorbed amount of Nd(III) by pristine mesoporous carbon is 3.4 mg/g, denoting that the MC-T00 adsorbed about three times higher Nd(III) compared to that of pristine mesoporous carbon. It is also interesting to note that there is no significant difference in the Nd(III) adsorbed amounts within different oligo grafted mesoporous carbons. In this regard, it should be emphasized that it was not possible for us to accurately determine the grafting density of different types of DNAs within the mesoporous carbon and a higher amount of phosphate groups essentially would enhance the adsorption of a REE, like Nd(III). Besides the grafting density, such phenomenon may also be explained from another hypothesis. We hypothesize that it may be caused by the sluggish diffusion of large chain oligos within the mesoporous carbon. Although a large unit of oligo contains a large number of phosphate

groups essentially suggesting elevated adsorption of Nd(III), a large-chain of oligo may also severely suffer from sluggish diffusion in the course of the grafting process. This slow diffusion may hinder the grafting of sufficient units of a long-chain oligo. On the other hand, although a short chain of oligo could be grafted more easily owing to the faster diffusion in the course of the reaction, the total number of phosphorous bearing units can be compensated by the smaller number of phosphate groups present in the shorter oligo. Nevertheless, the influence of oligo grafting on the mesoporous carbons is confirmed by the elevated Nd(III) adsorption compared to that of pristine mesoporous carbon. As the largest adsorbed amount of Nd(III) is shown by MC-T100, all the rest of the adsorption experiments were performed by this particular adsorbent only.

The equilibrium and kinetics of Nd(III) adsorption are shown in figure 5(a)-(c). As observed in figure 5(a), the equilibrium adsorbed amount of Nd(III) in MC-T100 increases monotonically with the increase in initial concentration, up to around 500 mg/L (ppm), without reaching the saturation level. Based on similar data, the adsorption isotherm of Nd(III) (figure 5(b)) showed a similar trend, the increase in adsorbed amounts with the increase in equilibrium concentration. The kinetics of adsorption is shown in figure 5(c). It is observed that Nd(III) adsorbed amount increases sharply within the first one hour and almost attained a plateau within a time interval of 3 hours. The kinetic equation, modeled by the pseudo-second-order kinetic equation, is given by

$$\frac{t}{q_t} = \frac{1}{k_2 q_e^2} + \left(\frac{1}{q_e}\right) t \dots (1)$$

Where, q_t is the adsorbed amount at time t and q_e is the equilibrium adsorbed amount. A linear regression analysis of $\frac{t}{q_t}$ versus t yields the pseudo-second-order rate constant, k_2 as $9.5 \times 10^{-4} \, \mathrm{g}^{-1} \mathrm{mg}^{-1} \mathrm{min}^{-1}$.

The distribution coefficient of adsorption (K_d) is defined as

$$K_d = \left(\frac{C_i - C_f}{C_f}\right) \left(\frac{V}{m}\right) \dots (2)$$

Where, C_i : Initial concentration, C_f : Final concentration, V: volume of the solution, and m: mass of the adsorbent. Distribution coefficient signifies the ratio of adsorbate concentration in the adsorbent over in the same concentration adsorption media (solution), when the system is in equilibrium. Unlike adsorbed amount, K_d also depends on the adsorption conditions, such as amount of solution employed and concentration of adsorbent in the mixture and therefore it provides more realistic understanding of adsorption behavior at a specific condition. The distribution coefficient K_d , as a function of the initial concentration of Nd(III) is shown in figure 6. As observed in figure 6, K_d attained the highest value in the lowest initial concentration of Nd(III), which is about 1100 mL/g and then decreases exponentially with the increase in Nd(III) concentration in the solution. It essentially suggests that Nd(III) adsorption is most effective in the lower dose. The adsorbed amount and distribution coefficient of Nd in MC-T100 is higher than other DNA-based materials, like salmon milt powder²⁰ or DNA-filter hybrid,²¹ and other sorbents, including freeze-dried powder of genetically engineered microbial strains¹⁹, EDTA and DTPA-functionalized chitosan²⁵ and ion-imprinted mesoporous silica³.

The pH dependency of Nd adsorption is shown in figure 7. The figure shows a noticeable general trend that the adsorbed amount is low at the lower pH and increases

rapidly at elevated pH. The distribution coefficient (K_d) calculated from the experimental conditions demonstrated similar trends. This type of pH dependency for REE adsorption was also for other types of sorbents, including, salmon milt powder²⁰, DNA-filter hybrid²¹, EDTA and DTPA functionalized chitosan²⁵, ion-imprinted mesoporous silica³ and magnetic nanohydroxyapatite²⁶. The pH dependency of the carbonaceous adsorbents is dictated by the surface charge, which is manifested by the chemical functionalities present on the surface of carbon. Majority of those functionalities include oxygen bearing functionalities that originatd from the carbon precursor, in addition to the DNA strands that have been on the mesoporous carbon surface. At a lower pH, more specifically, below the pH at point of zero charge, the carbon surface achieves positive charge^{27,28}. This positively charged surface electrostatically repels the positively charged cation, like Nd³⁺ in the course of adsorption resulting in lowering the adsorbed amount. As the pH increases, the carbon surface gradually becomes neutral thereby eliminating the electrostatic repulsion barrier and increasing the Nd³⁺ adsorption. At the highest pH of the experiment, more specifically, above the pH at point of zero charge, the carbon surface becomes negatively charged 27,28. This negatively charged surface electrostatically attracts positively charged Nd3+ ion thereby causing even higher adsorption of Nd(III). This type of pH dependency could provide an immediate notion that efficient adsorption could be performed at higher pH, whereas adsorbent can be regenerated at lower pH thereby demonstrating a pH-swing adsorption process.

The equilibrium adsorbed amounts of 16 rare earth elements (REEs), including Sc, Lu, Tm, Yb, Er, Ho, Tb, Dy, Y, Eu, Gd, Sm, Ce, Nd, Pr and La are shown in figure 8(a) and (b) for 1 ppm and 30 ppm of initial concentration with respect to each element, respectively. As expected, the equilibrium adsorbed amount is higher at the higher initial concentration of

30 ppm. An important observation that can be drawn from these plots is that scandium (Sc) and yttrium (Y) demonstrated significantly higher adsorbed amounts compared to the rest of the elements in these mixtures. It needs to be noted that these two elements do not belong to the lanthanide series and hence their chemical properties are not very similar to that of other rare earth elements (lanthanides). Within the lanthanides, a general observation is that the adsorbed amount of the elements increased with the increase in their corresponding atomic weight, starting from Lu to La. We also calculated the distribution coefficient (K_d) and the results are shown in figure 9(a)-(b). The distribution coefficient demonstrated a similar trend with that of pure Nd(III), i.e., K_d is higher at the lower initial concentration of REEs thereby suggesting that the adsorption is more effective in the lower concentration.

To further analyze the adsorption of different rare earth elements as a function of the atomic properties, we have plotted the adsorbed amounts (mg/g) as a function of metallic radii (pm) and the result is shown in figure 10(a). As this figure reveals, except Sc and Y (which are not the true lanthanides), a reasonably well linear trend $(R^2=0.83)$ is observed between the adsorbed amounts of lanthanides and the corresponding metallic radius of the atoms. In figure 10(b), we have plotted similar data, where the adsorbed amounts were represented as mmol/g. It is observed that the linear trend between adsorbed amounts and the metallic radius was even more prominent $(R^2=0.87)$. This type of behavior may be explained from the classical adsorption theory. If the pores of the adsorbent are too large or the size of adsorbate atom or ion is too small, the force field of adsorption originating from the opposite pore wall cannot reach the adsorbate and hence adsorption will become weak. In this case, as we find that the amount of REE adsorbed amount increased with the increase

in metallic radius, we can conclude that size of REEs with larger metallic radii are more appropriate to the size of active pores present in the adsorbate.

3.3 X-ray absorption spectroscopy (XAS)

The Nd L₃-edge XANES spectra for Nd in mesoporous carbon and solid Nd(NO₃)₃·6H₂O powder, normalized at the edge jump, are shown in figure 11. The extended X-ray absorption fine structure (EXAFS) spectra $\chi(k)k^2$ (k is the photoelectron wavenumber defined as $k = \sqrt{(2m_e/\hbar^2)(E-E_0)}$ where m_e is the electron mass, \hbar is the Planck's constant, and (E- E_0) is the photoelectron kinetic energy) were extracted and their Fourier transforms (FTs) were calculated using the 10% Gaussian window-function (figure 11). All reported FTs were not corrected for the backscattering phase shift of atoms so that the positions of all peaks are displaced to smaller distances relative to their crystallographic values. The E_0 value was selected at 6209 eV to best fit the theoretical energy scale calculated by the FEFF8.50L code^{29,30}. The first peak in FTs at about 1.9 Å corresponding to the first coordination shell of Nd atoms was isolated by the back-FT procedure in the range 1-2.8 Å.

The backscattering amplitude and phase shift functions for Nd-O atom pair were calculated using ab initio self-consistent real-space multiple-scattering FEFF8.50L code^{29,30}. The scattering potential and partial phase shifts were calculated within the muffin-tin (MT) approximation 29,30 for a cluster with a radius of 8 Å, centered at the absorbing Nd atom. The cluster was constructed from the crystallographic structure of $Nd(NO_3)_3 \cdot 6H_2O^{-31}$. The photoelectron inelastic losses were accounted for within the one-plasmon approximation using the complex exchange-correlation Hedin-Lundqvist potential³². The Nd L₃-edge EXAFS

spectra were analyzed using a conventional procedure³³. Multiple-scattering analysis of $Nd(NO_3)_{3.6}H_2O$ (figure S1 and figure S2) is given and discussed in Supporting information.

Normalized Nd L₃-edge XANES spectra for Nd in mesoporous carbon and solid $Nd(NO_3)_3 \cdot 6H_2O$ powder are compared in figure 11. The position of the absorption edge coincides well in both compounds indicating the same (3+) oxidation state of neodymium ions. The so-called "white line" (WL), i.e., a strong absorption resonance located just above the absorption edge at about 6210 eV, dominates both spectra. It is due to the electric-dipole allowed (Δl =+1, l is the orbital angular momentum) transition from the core state $2p_{3/2}(Nd)$ to quasi bound states having the 5d(Nd) atomic character³⁴.

It was suggested earlier 35 that the intensity of WL at the Nd $_{2,3}$ -edges correlates with the partially covalent character of its chemical bonds with ligands. The 4f electrons in Nd $^{3+}$ complexes are not completely localized and interact weakly with ligand orbitals 36,37 . Therefore, the back-charge transfer from ligands to partly filled 4f (Nd) orbitals occurs, leading to an increase in the screening effect of the excited photoelectron in the 5d-like state. As a result, the photoelectron wave function becomes more localized that promotes an increase of the transition matrix element between the $^{2p_{3/2}}$ (Nd) core level and the final state and, ultimately, raises the WL intensity 35 . Based on this model, the comparison of the WL intensities in figure 11 suggests that the bonding between Nd $^{3+}$ ions and surrounding ligands is slightly more covalent, i.e. the bonds are stronger, in porous carbon. This result correlates well with a smaller radius of the first coordination shell of Nd $^{3+}$ ions in porous carbon, being evident from a small, but detectable, shift of the first oscillation maximum at 6240 eV to higher energies.

More detailed information on the local atomic structure around neodymium ions can be extracted from the analysis of EXAFS. The experimental Nd L₃-edge EXAFS spectra $\chi(k)k^2$ and their Fourier transforms (FTs) are shown in figure 12 together with the contributions from the first coordination shells isolated using the back-FT procedure. The EXAFS spectra of both compounds include mainly low-frequency signals from the first shell (the peak at about 2 Å in FTs), whereas the outer coordination shell contributions are weak and appear as several small peaks above 3 Å (figure 12(b)). Strong damping of the total and first-shell EXAFS signals at large k-values is evident and indicates the presence of a large disorder. The first peak in FTs is close in the two compounds, however, it is slightly shifted to lower distances in porous carbon due to the lower frequency of the EXAFS oscillations (figure 12(a)).

The analysis of the first coordination shell EXAFS $\chi(k)k^2$ was performed in the single-scattering approximation. ^{29,30} based on the EXAFS equation for a group of N atoms located at the distance R around the absorbing neodymium atom

$$\chi(k) = NS_0^2 \frac{f^l(\pi, k, R)}{kR^2} \sin\left[2kR - \frac{4}{3}C_3k^3 + \psi^l(\pi, k, R) + 2\delta_c^l(k)\right] e^{-2k^2\sigma^2} e^{-2R/\lambda(k)}.$$
 (3)

Here N is the coordination number, S_0^2 is a many-body reduction factor accounting for amplitude damping due to multi-electron effects (intrinsic losses), $f^l(\pi, k, R)$ and $\psi^l(\pi, k, R)$ are the backscattering amplitude and phase shift of the photoelectron by the neighboring oxygen atoms, $2\delta_c^l(k)$ is the final-state phase shift at the absorbing neodymium atom, and $\lambda(k)$ is the energy-dependent mean free path (MFP) of the photoelectron. The last four

functions were calculated by the FEFF8.50L code^{29,30}. The exponential term $e^{-2k^2\sigma^2}$ takes into account the effects of thermal disorder σ_{th}^2 within the harmonic approximation and static disorder σ_{st}^2 described by a Gaussian distribution with $\sigma^2 = \sigma_{th}^2 + \sigma_{st}^2$ (model #1). The parameter σ^2 is called the Debye-Waller factor or mean-square relative displacement (MSRD) for the Nd-O atom pair. When a distance distribution deviates slightly from the Gaussian shape, for example, for anharmonic vibrations or specific static disorder, the third cumulant C_3 can be introduced into the model (model #2).

The results of the best-fit analysis using models #1 and #2 are reported in figure 13. While both models show rather good agreement with the experimental EXAFS of the first coordination shell, nevertheless, model #2 gives slightly better agreement at k > 5.5 Å⁻¹. The inclusion of the third cumulant C_3 allows us to account for a weak asymmetry of the first shell peak in FTs and, thus, give slightly better overall agreement. The obtained values of the structural parameters are given in table 1. Note that there is some correlation between the values of the interatomic distance and the third cumulant since both parameters influence the EXAFS frequency. Also, the reliable experimental EXAFS data are available in the limited k-space range up to 7.5 Å⁻¹ due to a set of glitches located at higher wavenumbers k.

Table 1. Structural parameters obtained from the best-fit analysis of the first coordination shell EXAFS for Nd in mesoporous carbon and $Nd(NO_3)_3 \cdot 6H_2O$.

	Nd(NO3)3-6H2O		Nd in mesoporous carbon	
	Model #1	Model #2	Model #1	Model #2
NS_0^2	7.5 ± 0.9	7.4 ± 0.8	8.9 ± 0.8	8.9 ± 0.8
R (Å)	2.48 ± 0.02	2.45 ± 0.02	2.45 ± 0.02	2.41 ± 0.02
σ^2 (Å ²)	0.008 ± 0.002	0.008 ± 0.002	0.011 ± 0.002	0.011 ± 0.002
C_3 (Å ³)		-0.0020 ± 0.0007		$\textbf{-0.0024} \pm 0.0007$

Before discussing the obtained results, one should point out that the local environment of neodymium ions in the reference compound $Nd(NO_3)_3 \cdot 6H_2O$ Error! Bookmark not defined. is very distorted. Neodymium is coordinated to 10 oxygen atoms, belonging to three NO_3 groups and four H_2O molecules. As a result, the Nd-O distances range from 2.43 Å to 2.72 Å with the mean value of about 2.52 Å. This broad distribution of the interatomic distances is the origin of the EXAFS damping at the large k-values leading to the large value of the MSRD factor for Nd-O bonds. Note also that in such a situation EXAFS is more sensitive to the shortest bonds since they give a stronger contribution to the total signal.

A comparison of the structural parameters obtained within the same model indicates that the main difference between the local environment of Nd^{3+} ions in the two compounds is related to the mean interatomic distance Nd-O, which is shorter by about 0.03-0.04 Å in porous carbon. This result correlates well with the behavior of the Nd L_3 -edge XANES in figure 11. All other structural parameters are close taking into account the errors. The

correlations between R and C_3 as well as between NS_0^2 and σ^2 are well visible and are due to the short range of the EXAFS spectra used in the analysis.

4. Conclusions

In this study, we have successfully synthesized DNA grafted mesoporous carbons with different strains of single-stranded DNA. Pure Nd(III) adsorption study confirmed that adsorbed amount increased significantly in DNA grafted carbons compared to that of pristine mesoporous carbon. The values of the distribution coefficient signified that adsorption is more effective in the lower initial dose of the rare earth elements. The experiments also revealed that the adsorption amount is low in the low pH, but increases at the high pH that may be attributed to the surface charge of porous carbons. Adsorption experiments with a mixture of REEs confirmed that the adsorbed amount increases with the increase in atomic weight and metallic radii of the lanthanides in a linear fashion. The Nd L₃-edge XANES confirms the 3+ oxidation state of neodymium ions in porous carbon. The comparative EXAFS analysis suggests that the first coordination shell of Nd3+ ions in porous carbon and in the reference compound $Nd(NO_3)_3 \cdot 6H_2O$ is rather similar being strongly distorted and composed of about 10 oxygen atoms. However, the mean Nd-O distance for Nd(III) adsorbed on P and O functionalized porous carbon is slightly shorter by about 0.03-0.04 Å than in Nd(NO₃)₃·6H₂O. This fact can be explained by the local structure relaxation within Ndcomplexes located at the surface of porous carbon. Besides, the shortening of the mean Nd-O distance leads to a slight increase of bond covalency observed as an increase of the white line intensity in XANES.

Supporting Information

Experimental and calculated Nd L_3 -edge EXAFS spectra and their FTs, Calculated Nd L_3 -edge EXAFS spectra and their FTs, Single-scattering (SS) and multiple-scattering (MS) contributions.

Acknowledgements

This work has been funded by National Science Foundation (NSF) with the grant number 1837202. C. E. U. acknowledges support from School of Engineering of Widener University. This research used beamline QAS of the National Synchrotron Light Source II, a U.S. Department of Energy (DOE) Office of Science User Facility operated for the DOE Office of Science by Brookhaven National Laboratory under Contract No. DE-SC001270. The authors acknowledge Dr. Jamie Morris of Sing center of nanotechnology of University of Pennsylvania for assisting in SEM-EDX imaging.

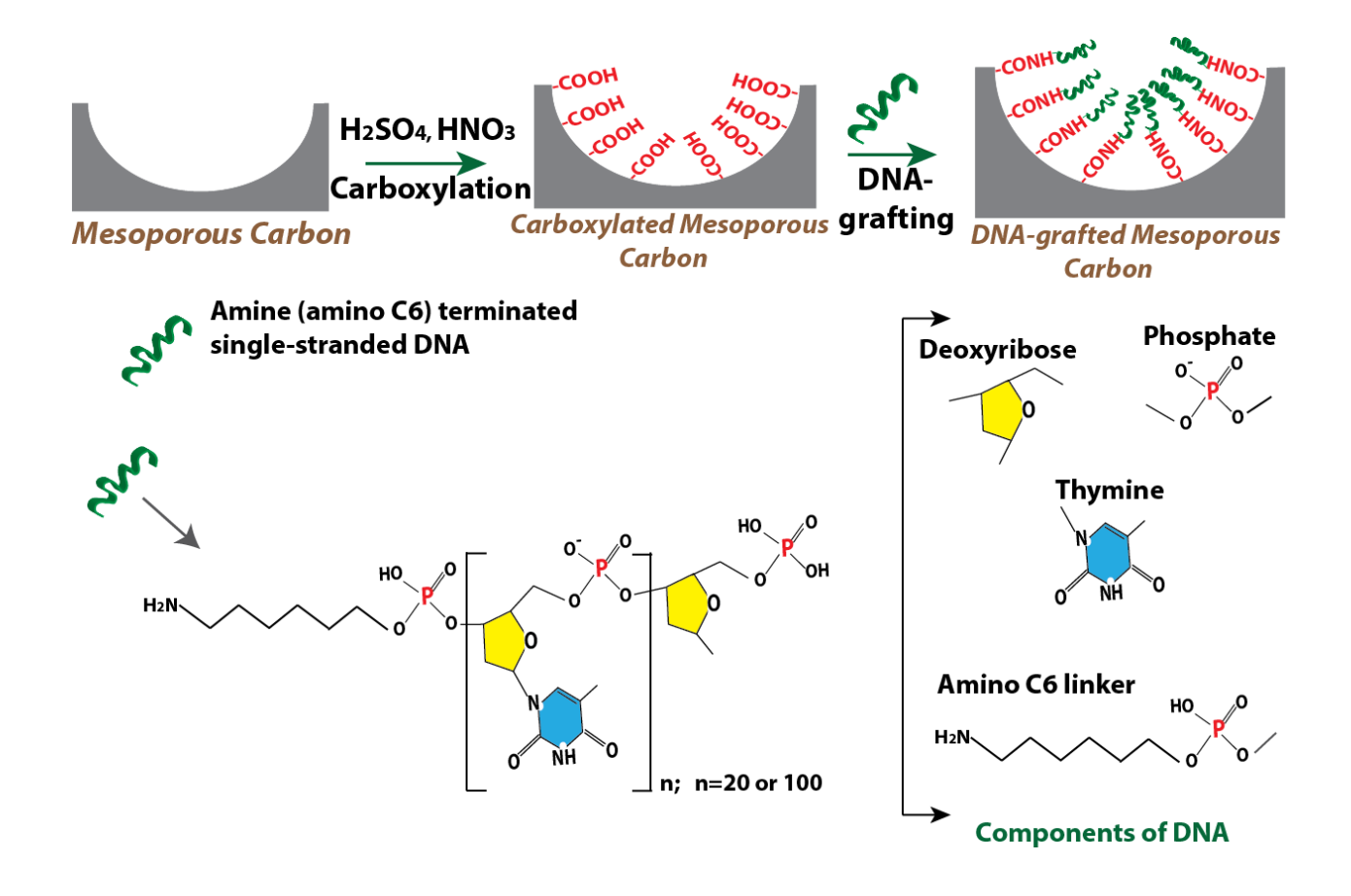


Figure 1. Overall schematic of the synthesis of DNA functionalized mesoporous carbons

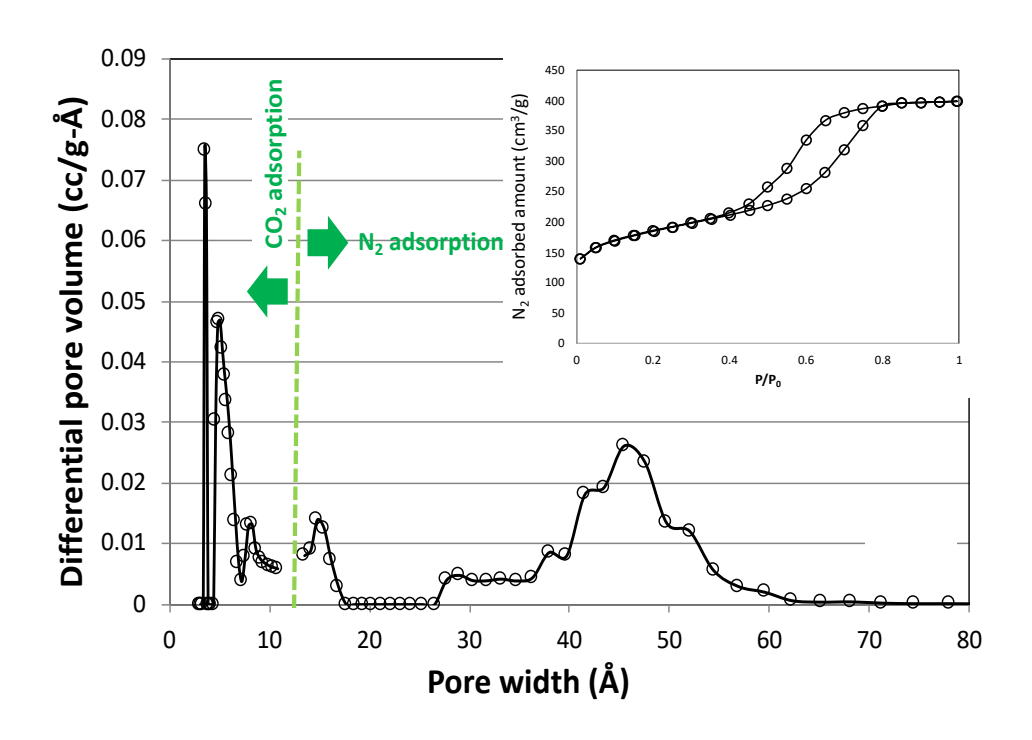


Figure 2. The pore size distribution of mesoporous carbon (inset: N_2 adsorption-desorption plot at 77 K).

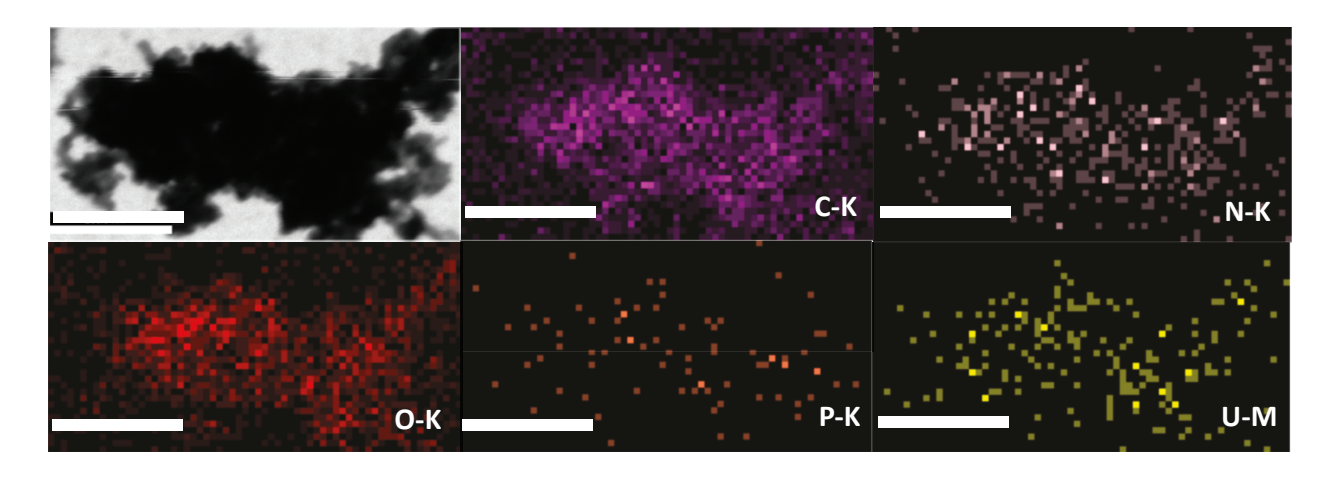


Figure 3. SEM image (a) and EDX mapping for carbon (b), nitrogen (c), oxygen (d), phosphorous (e) and uranium (f). All the scale bars reprent 200 nm

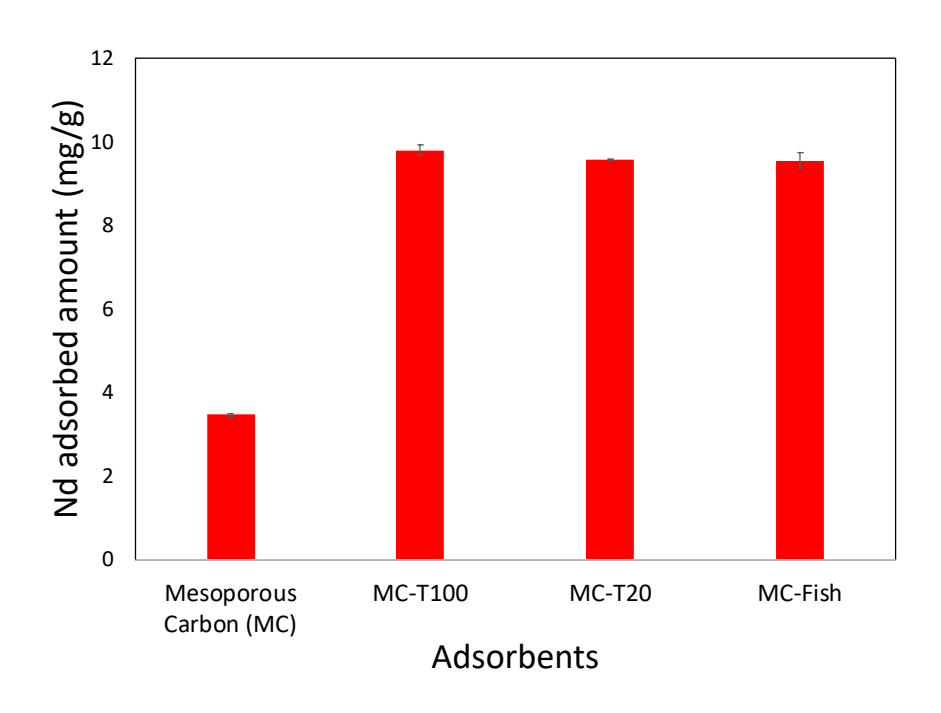


Figure 4. Results of the best adsorbent analysis.

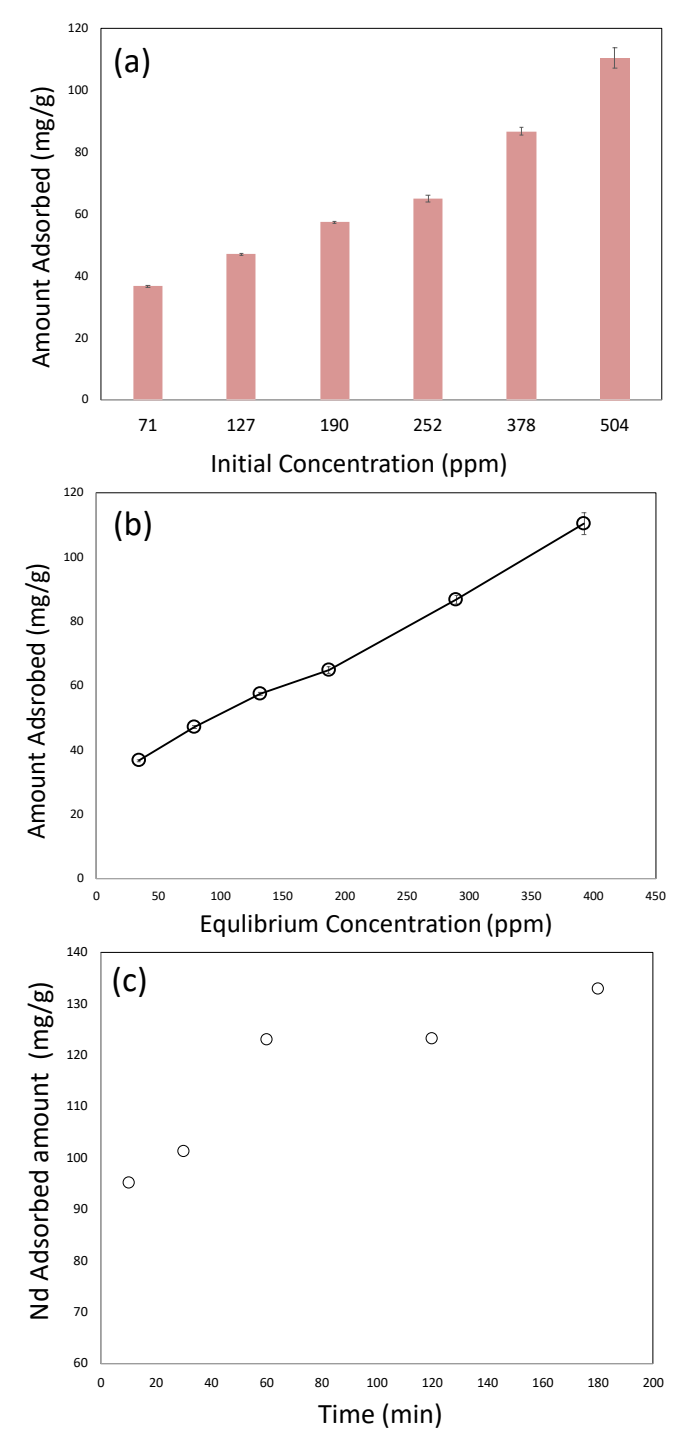


Figure 5. Nd (III) adsorbed amounts as a function of initial concentration (a), equilibrium concentration (b) and time (c). For (a) and (b), 25 mg adsorbent (MC-T100) was employed in 25 mL Nd(NO₃)₃ solution. For (c), 25 mg adsorbent (MC-T100) was employed in 25 mL $500 \, mg/L \, \text{Nd}(\text{NO}_3)_3 \, \text{solution}$

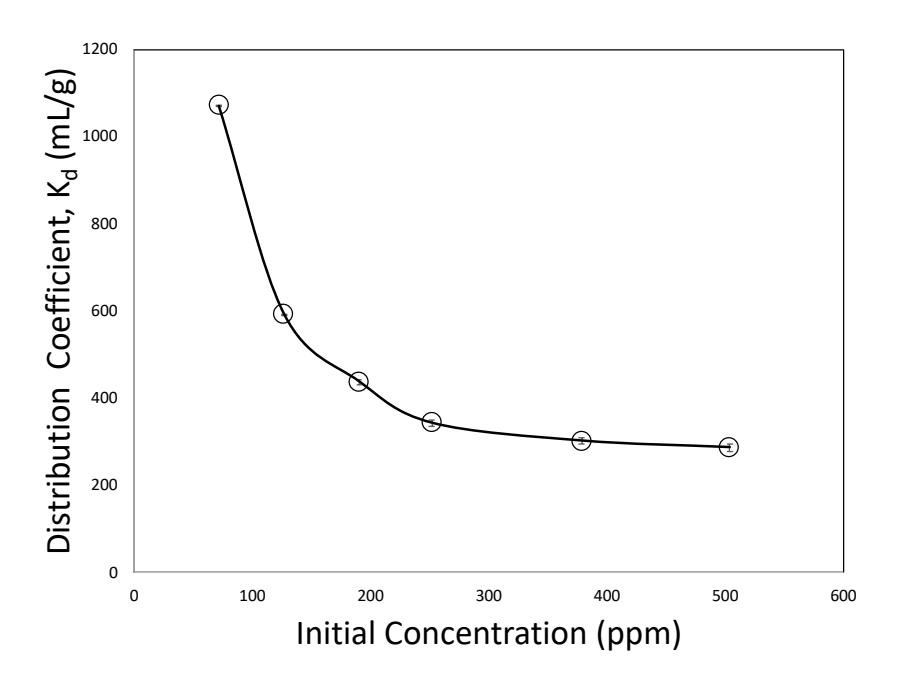


Figure 6. Distribution coefficient, K_d of Nd(III) as a function of initial concentration. For each data point, 25 mg adsorbent (MC-T100) was employed in 25 mL Nd(NO₃)₃ solution.

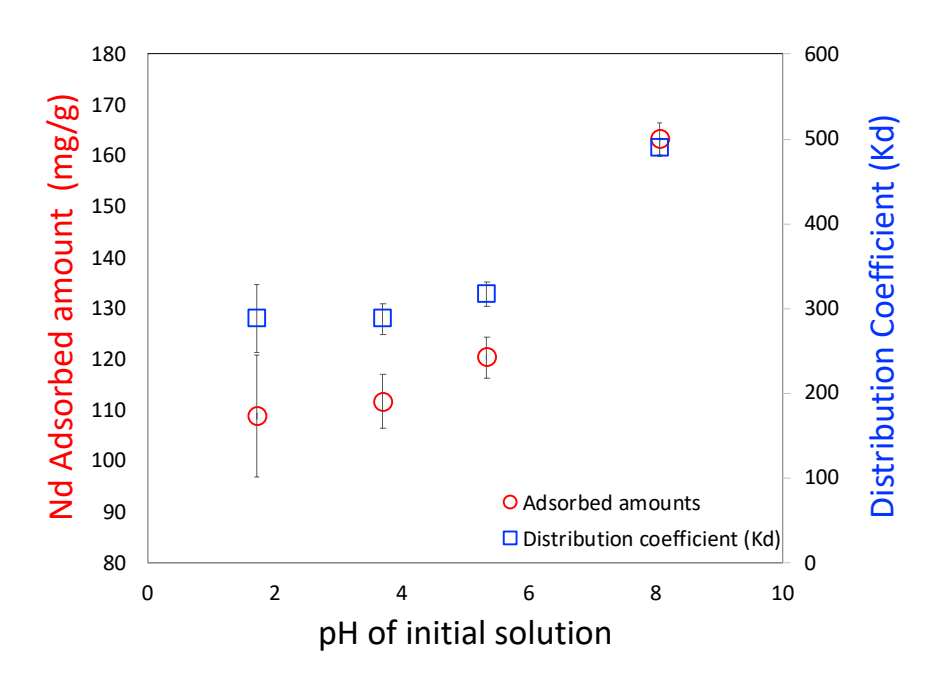


Figure 7. Influence of solution pH on the adsorption of Nd(III). 25 mg adsorbent (MC-T100) was employed in 25 mL 500 mg/L Nd(NO₃)₃ solution

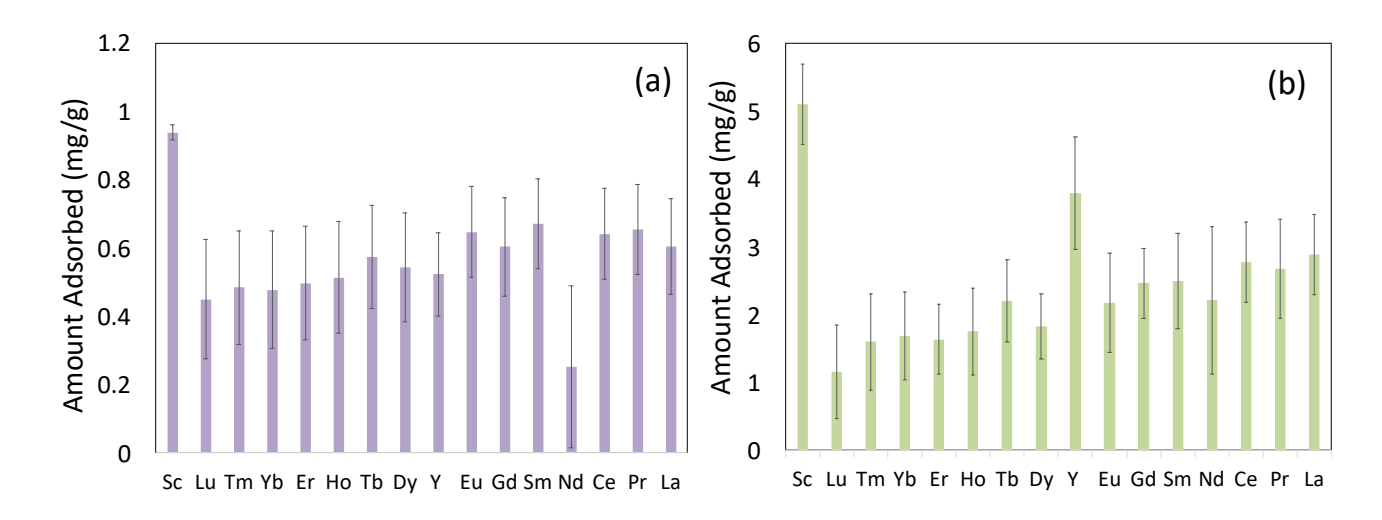


Figure 8. REE mixture adsorption with the initial concentration of 1 ppm (a) and 30 ppm (b).

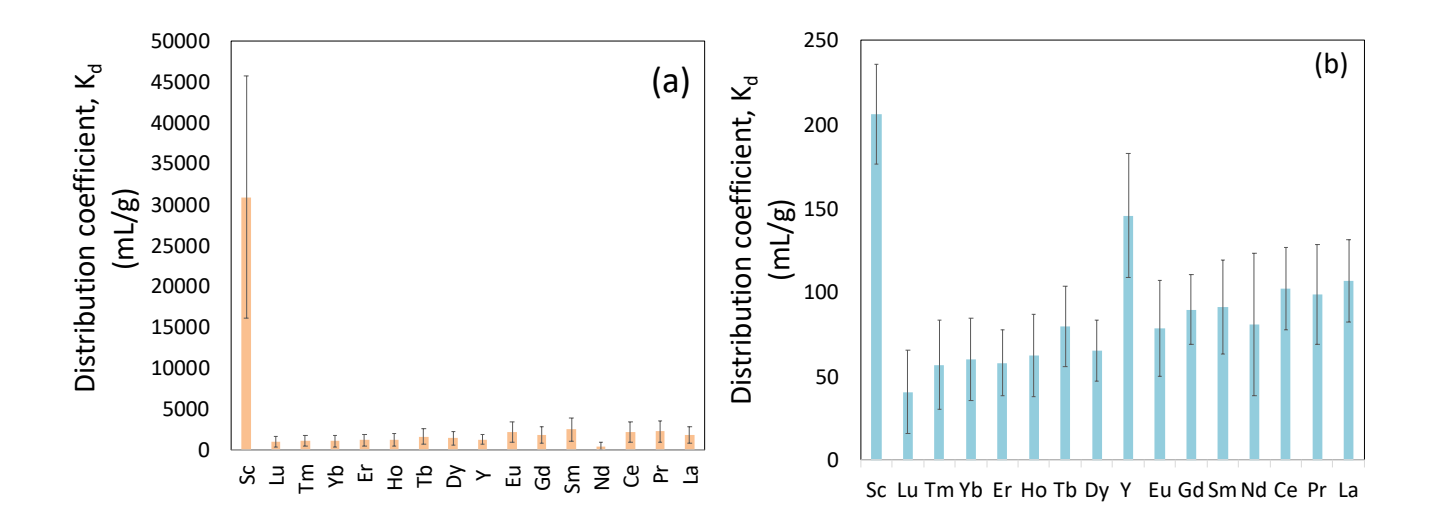


Figure 9. Distribution coefficient, K_d for REE mixture adsorption with initial concentration 1 ppm (a) and 30 ppm (b).

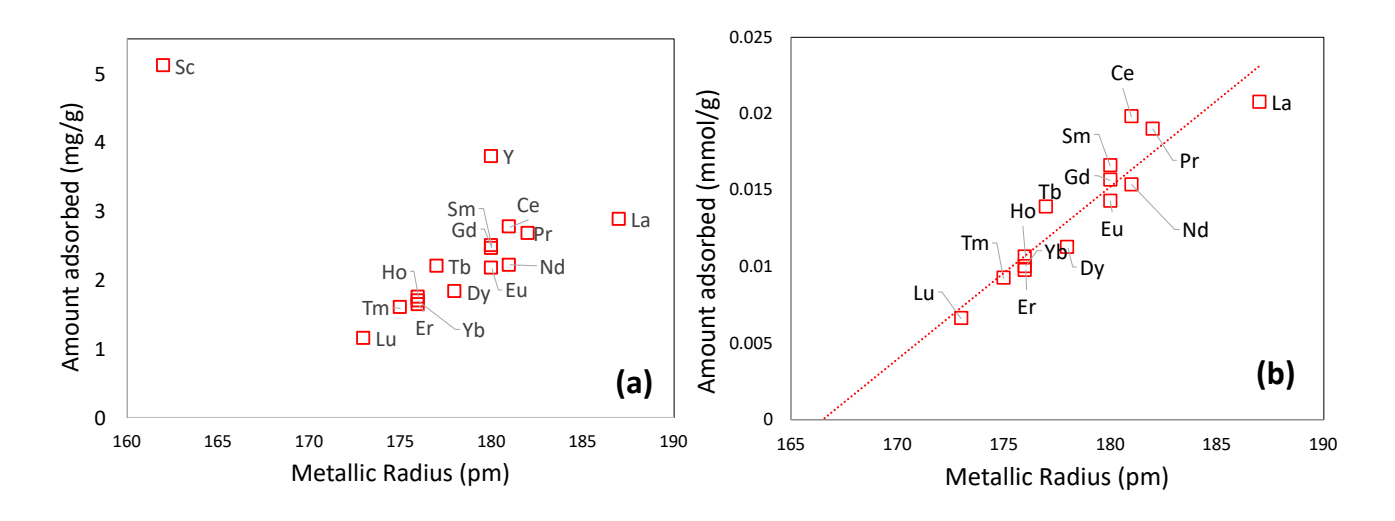


Figure 10. Linear relationship between adsorbed amount of REE and metallic radius for mass basis (a) and mole basis (b) adsorption.

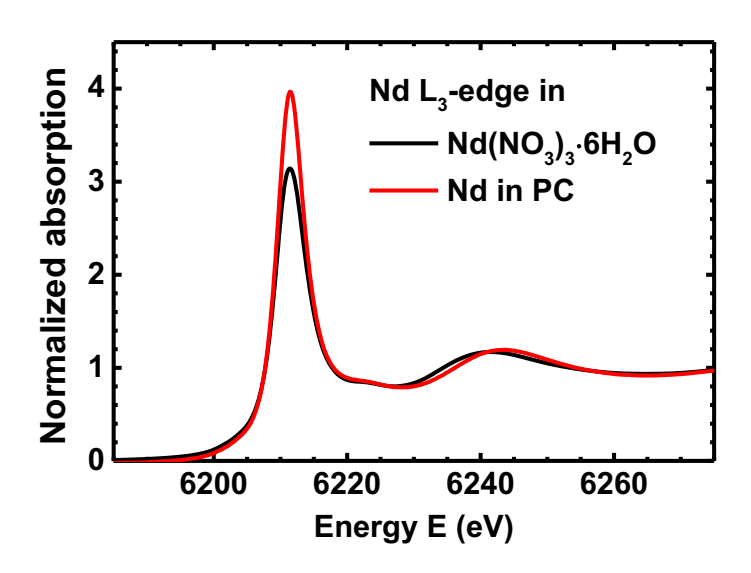


Figure 11. Normalized Nd L_3 -edge XANES spectra of $Nd(NO_3)_3 \cdot 6H_2O$ and Nd adsorbed on P and O functionalized porous carbon (PC, MC-T100).

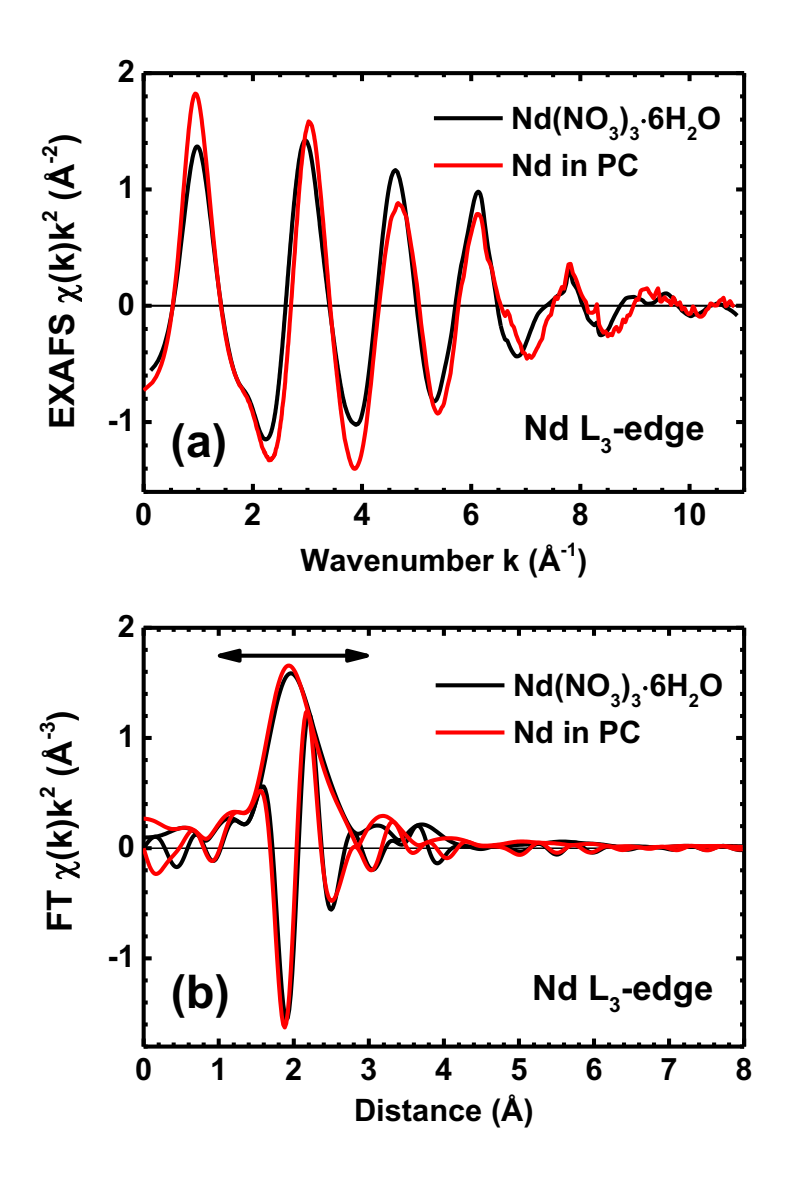


Figure 12. (a) Experimental Nd L₃-edge EXAFS spectra $\chi(k)k^2$ and (b) their Fourier transforms (FTs) for $Nd(NO_3)_3 \cdot 6H_2O$ and Nd adsorbed on P and O functionalized porous carbon (PC, MC-T100). FT modulus and imaginary parts are shown in (b). Arrow indicates the range of the first coordination shell of neodymium.

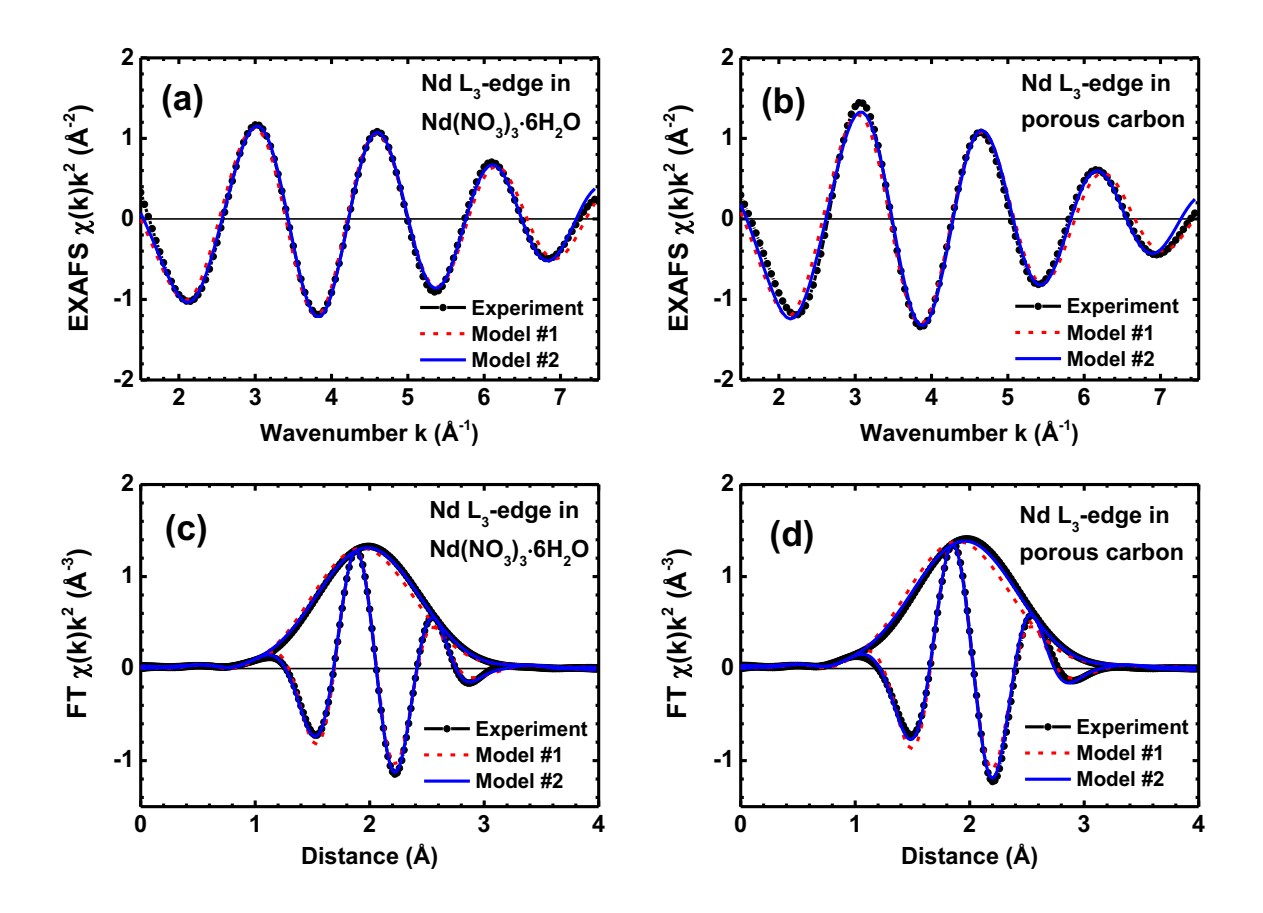


Figure 13. Comparison of the experimental and best-fit EXAFS spectra $\chi(k)k^2$ (a,b) and their FTs (c,d) for $Nd(NO_3)_3 \cdot 6H_2O$ (a,c) and Nd adsorbed on P and O functionalized porous carbon, MC-T100 (b,d). Dashed curves are the Gaussian model (model #1), solid lines are the cumulant model (model #2).

References

- ² Das, N.; Das, D. Recovery Of Rare Earth Metals Through Biosorption: An Overview. *J. Rare Earths.* 2013, 31, 933-943.
- ³ Zheng, X.; Liu, E.; Zhang, F.; Yan, Y.; Pan, J. Efficient Adsorption and Separation of Dysprosium from Ndfeb Magnets in An Acidic System by Ion Imprinted Mesoporous Silica Sealed in a Dialysis Bag, *Green Chem.* 2016, 18, 5031–5040.
- ⁴ Alonso, E.; Sherman, A.M.; Wallington, T.J.; Everson, M.P.; Field, F.R.; Roth, R.; Kirchain, R.E. Evaluating Rare Earth Element Availability: A Case with Revolutionary Demand from Clean Technologies. *Environ. Sci. Technol.* 2012, 46, 3406–3414.
- ⁵ Sprecher, B.; Kleijn, R.; Kramer, G.J. Recycling Potential of Neodymium: The Case of Computer Hard Disk Drives. *Environ. Sci. Technol.* 2014, 48, 9506–9513.
- ⁶ Sengupta, J.G. Determination of Scandium, Yttrium and Lanthanides in Silicate Rocks and Four New Canadian Iron Formation Reference Materials by Flame Atomic-Absorption Spectrometry with Micro Sample Injection. *Talanta* 1984, 31,1045-1051.
- ⁷ Kim, J.S.; Lee, C.H.; Han, S.H.; Suh, M.Y. Studies on Complexation and Solvent Extraction of Lanthanides in the Presence Of Diaza-18-Crown-6-Di-Isopropionic Acid. *Talanta* 1997, 45, 437-444.
- ⁸ Xiong, C.H.; Liu, X.Z.; Yao, C.P. Effect of pH on Sorption for REE(III) and Sorption Behaviors of Sm(III) By D152 Resin. *J. Rare Earths*. 2008, 26, 851-856.
- ⁹ Xiong, C.H. Sorption Behavior of D155 Resin for Ce(III). *Ind. J. Chem.* 2008, 47A, 1377-1380.

¹ Anastopoulosa, I.; Bhatnagar, A.; Limac, E.C. Adsorption Of Rare Earth Metals: A Review of Recent Literature. *J. Molecular Liquids*. 2016, 221, 954–962.

¹⁰ Zhu, Y.; Zheng, Y.; Wang, A. A Simple Approach to Fabricate Granular Adsorbent for Adsorption of Rare Elements. *Int. J. Biol. Macromol.* 2015, 72, 410–420.

- ¹¹ Xie, F; Zhang, T. A.; Dreisinger, D.; Doyle, F. A Critical Review on Solvent Extraction of Rare Earths from Aqueous Solutions. *Minerals Engg.* 2014, 56, 10–28.
- ¹² Yao, C.P. Adsorption and Desorption Properties of D151 Resin for Ce(III). *J. Rare Earths*. 2010, 28, 183-188.
- ¹³ Ritcey, G.M.; Ashbrook, A.W. Solvent Extraction: Principle and Applications to Process Metallurgy, Part I. Amsterdam. *Elsevier Press.* 1984, 603.
- ¹⁴ Samuelson, O. Ion Exchangers in Analytical Chemistry. *John Wiley*. 1972, 415.
- ¹⁵ Xiong, C.H.; Zheng, Z.W. Evaluation Of D113 Cation Exchange Resin for The Removal of Eu(III) from Aqueous Solution. *J. Rare Earths.* 2010, 28, 862-867.
- ¹⁶ Park, H-J.; Tavlarides, L.L. Adsorption of Neodymium(III) from Aqueous Solutions Using a Phosphorus Functionalized Adsorbent, *Ind. Eng. Chem. Res.* 2010, 49, 12567–12575.
- ¹⁷ Saha, D.; Akkoyunlu, S.D.; Thorpe, R.; Hensley, D.K.; Chen, J. Adsorptive Recovery of Neodymium and Dysprosium in Phosphorous Functionalized Nanoporous Carbon. *J. Environmental Chemical Engineering*, 2017, 5, 4684-4692.
- ¹⁸ Takahashi, Y.; Châtellier, X.; Hattori, K.H.; Kato, K.; Fortin, D. Adsorption of Rare Earth Elements onto Bacterial Cell Walls and Its Implication for REE Sorption onto Natural Microbial Mats. *Chemical Geology*. 2005, 219, 53–67
- ¹⁹ Moriwaki, H.; Masuda, R.; Yamazaki, Y.; Horiuchi, K.; Miyashita, M.; Kasahara, J.; Tanaka, T.; Yamamoto, H. Application of Freeze-Dried Powders of Genetically Engineered Microbial Strains as Adsorbents for Rare Earth Metal Ions, *ACS Appl. Mater. Interfaces.* 2016, 8, 26524–26531.

²⁰ Takahashi, Y.; Kondo, K.; Miyaji, A.; Watanabe, Y.; Fan, Q.; Honma, T.; Tanaka, K. Recovery and Separation of Rare Earth Elements Using Salmon Milt. *Plos One* 2014, 9, e114858.

- ²¹ Takahashi, Y.; Kondo, K.; Miyaji, A.; Umeo, A.M.; Honma, T.; Asaoka, S. Recovery and Separation of Rare Earth Elements Using Columns Loaded with DNA-filter Hybrid. *Analytical sciences*. 2012, 28, 985-992.
- ²² Gencoglu, M.F.; Spurri, A.; Franko, M.; Chen, J.; Hensley, D.K.; Heldt, C.; Saha, D. Biocompatibility of Soft-Templated Mesoporous Carbons, *ACS Appl. Mater Interfaces*, 2014, vol. 6, no. 17, pp 15068-15077.
- ²³ Saha, D.; Tom, B.; Fieback, T. Characteristics of Methane Adsorption in Micro-Mesoporous Carbons in Low and Ultra-High Pressure, *Energy Technology*, 2016, 4, 1392-1400.
- ²⁴ Saha, D.; Richards, C.P.; Haines, R.G.; D'Alessandro, N.D.; Kienbaum, M.J.; Griffaton, C.A. Competitive Adsorption of Lead in Sulfur and Iron Dual-Doped Mesoporous Carbons, *Molecules* 2019, vol. 25 pp 403.
- ²⁵ Roosen, J.; Binnemans, K. Adsorption and Chromatographic Separation of Rare Earths with EDTA- And DTPA-Functionalized Chitosan Biopolymers, J. Mater. Chem. A, 2014, 2, 1530–1540.
- ²⁶ Gok, C. Neodymium and Samarium Recovery By Magnetic Nano-Hydroxyapatite, J Radioanal Nucl Chem (2014) 301:641–651.
- ²⁷ Saha, D.; Barakat, S.; Van Bramer, S.; Nelson, K.A.; Hensley, D.K.; Chen, J. Non-Competitive and Competitive Adsorption of Heavy Metals in Sulfur-Functionalized Ordered Mesoporous Carbon, *ACS Applied Materials and Interfaces*, 2016, 8, 34132–34142.
- ²⁸ Kabiri, S.; Tran, D. N. H.; Azari, S.; Losic, D. Graphene-Diatom Silica Aerogels For Efficient Removal Of Mercury Ions From Water. ACS Appl. Mater. Interfaces 2015, 7, 11815–11823.

- ²⁹ Ankudinov, A.L.; Ravel, B.; Rehr, J.J.; Conradson, S.D. Real-Space Multiple-Scattering Calculation and Interpretation of X-Ray-Absorption Near-Edge Structure, *Phys. Rev. B*, 1998, 58, 7565-7576.
- ³⁰ Rehr, J.J.; Albers, R.C. Theoretical Approaches to X-Ray Absorption Fine Structure, *Rev. Mod. Phys.*, 2000, 72, 621-654.
- ³¹ Rogers, D.J.; Taylor, N.J.; Toogood, G.E.; Tetraaquatrinitratoneodymium(III) dihydrate, [Nd(NO₃)₃(H₂O)₄]·2H₂O, *Acta Cryst. C*, 1983, 39, 939-941.
- ³² Hedin, L.; Lundqvist, S. Explicit Local Exchange-Correlation Potentials, *J. Phys. C: Solid State Phys.*, 1971, 4, 2064-2083.
- ³³ Kuzmin, A.; Chaboy, J. EXAFS and XANES Analysis of Oxides at the Nanoscale, *IUCrJ*, 2014, 1, 571-589.
- ³⁴ Rocca, F.; Kuzmin, A.; Purans, J.; Mariotto, G. X-Ray Absorption Spectroscopy Study af a Nd³⁺-Exchanged β"-Alumina Crystal, *Phys. Rev. B*, 1994, 50, 6662-6672.
- ³⁵ Rao, K.J.; Wong, J.; Weber, M.J. Bonding And Structure of Nd³⁺ In Bef₂ Glass by XANES and EXAFS Spectroscopy, *J. Chem. Phys.*, 1983, 78, 6228-6237.
- Tandon, S.P.; Mehta, P.C. Study of Some Nd³⁺ Complexes: Interelectronic Repulsion, Spin–Orbit Interaction, Bonding, and Electronic Energy Levels, *J. Chem. Phys.*, 1970, 52, 4896-4902.
 Ryzhkov, M.V.; Gubanov, V.A.; Teterin, Yu.A.; Baev, A.S. Electronic Structure, Chemical Bonding and X-Ray Photoelectron Spectra of Light Rare-Earth Oxides, *Z. Phys. B*, 1985, 59, 1-

TOC Graphic

6.

